X-ray-diffraction measurements from imperfect GaAs crystals: Evidence for near-surface defects

R. Bloch, D. Bahr, J. Olde, L. Brügemann, and W. Press
Institut für Experimentalphysik, Christian-Albrechts-Universität Kiel, Leibnizstrasse 19, D-2300 Kiel 1, Federal Republic of Germany

(Received 22 December 1989; revised manuscript received 26 March 1990)

Gallium arsenide crystals with orientations $[\bar{1}\,\bar{1}\,\bar{1}]$ and [111] were measured with use of a three-crystal x-ray diffractometer. Owing to the preparation of the surface of the substrates and the growing conditions using molecular-beam epitaxy (MBE), a concentration of large defect clusters of several parts per million in the MBE-grown layers results. These defects cause considerable diffuse scattering, which is visible around the reciprocal-lattice points. Even for evaporated MBE layers with thicknesses of only about 3000 Å, diffusely scattered intensity can be detected.

I. INTRODUCTION

X-ray diffuse scattering has been used very successfully to study defects in crystals. There exist experimental studies of interstitials in neutron-irradiated silicon,[1,2] electron-irradiated aluminum,[3] dislocation loops in copper,[4] and defects in float-zone (FZ) silicon.[5] Recently Czochralski-grown silicon with oxide clusters has been studied with small-angle neutron scattering.[6] The theory of diffuse x-ray scattering has been developed by Krivoglaz,[7] Trinkaus,[8,9] Dederichs,[10,11] and Dietrich and Fenzl.[12,13] All these works are concerned with defects in the bulk of the crystal. In the last years the interest has shifted to scattering from defects in thin films and surface layers.[14] Grotehans *et al.*[15] investigated the diffuse scattering from arsenide-ion-implanted silicon single crystals using grazing-incidence diffraction to obtain information from near-surface regions.

In this study we report measurements performed with polished gallium arsenide (GaAs) wafers with nearly perfect surfaces and molecular-beam-epitaxially (MBE) -grown GaAs layers.

The MBE layers were characterized with reflection high-energy electron diffraction (RHEED) and were examined by angle-resolved photoemission spectroscopy (ARPES) in ultrahigh vacuum (UHV) in order to determine the electronic band structure. To obtain additional information about the MBE layers, x-ray-diffraction measurements were made using conventional diffraction techniques. Initially we had been mainly interested in investigating the roughness of surfaces and layer-substrate interfaces and the crystalline structure of the MBE layers. But as the x-ray-diffraction measurements showed intense diffuse scattering around the Bragg reflection, our main interest shifted towards measuring and interpreting this diffuse scattering. From the diffusely scattered intensity we can learn about the defect structure, especially of the MBE layers. In this paper we present the investigation of four different GaAs(111) samples. A polished GaAs$(\bar{1}\,\bar{1}\,\bar{1})$ wafer (sample A) is used as a reference for the determination of the diffuse scattered intensity from the samples. A polished GaAs(111) wafer (sample B) is an example for a typical substrate for MBE-grown samples. The other two samples (C,D) are MBE-grown GaAs(111) layers.

After treatment in UHV the samples were kept in a surrounding at atmospheric pressure for a few weeks. At the time we examined the samples with x-ray diffraction, the surfaces had acquired a milky shining appearance. Obviously, the samples were no longer in the well-defined state they were in at the time of preparation and during spectroscopical measurements.

Samples "aged" in such a manner are less suited to show and test the possibilities of MBE, but are a stringent test for the possibilities of x-ray-diffraction techniques. It is difficult to give a thorough definition of the initial state so we do not expect a fully satisfactory and exhaustive interpretation. A few unsolved problems are left concerning the change in appearance of the samples at atmospheric pressure.

First of all, there will be a change in the roughness of the surfaces due to the influence of oxidation. We do not expect oxygen to have diffused deeply into the layer because no heat treatment took place after removal from UHV. So below a distorted layer of several Å, the samples probably are unaffected.

II. THEORY

We will not give a complete account of the theory of diffuse x-ray scattering from defects: Several excellent papers give a thorough discussion of this theory.[7–14] For a better understanding of our analysis it seems necessary, however, to give an outline of the theory.

In the kinematical approximation the scattered amplitude for x-ray diffraction from crystalline samples is

 ©1990 The American Physical Society

$$F(\mathbf{Q})=\sum_m \sum_n f_{mn}\exp(i\mathbf{Q}\cdot\mathbf{R}_{mn})=\sum_m f_m \exp(i\mathbf{Q}\cdot\mathbf{R}_m)\ . \quad (1)$$

f_{mn} is the atomic form factor and $\mathbf{R}_{mn}$ is the position of atom n in the mth unit cell. The first summation is extended over the whole crystal, the second over the unit cell. Thus f_m is the structure factor and $\mathbf{R}_m$ is the position of the unit cell m.

The momentum transfer $\mathbf{Q}$ is defined by

$$\mathbf{Q}=\mathbf{k}_f-\mathbf{k}_i \quad \text{with} |\mathbf{Q}|=4\pi\sin\theta/\lambda\ . \quad (2)$$

The subscripts i and f stand for the initial and final wave vector $\mathbf{k}$ of the incident and scattered x rays, respectively. λ is the wavelength of the x-rays and 2θ the scattering angle.

The statistically distributed defects cause static displacements of the atoms. Due to these static displacements the unit-cell positions $\mathbf{R}_m$ fluctuate with $\mathbf{u}_m$ around the average position $\langle \mathbf{R}_m \rangle$:

$$\mathbf{R}_m=\langle \mathbf{R}_m \rangle+\mathbf{u}_m\ . \quad (3)$$

For simplification, $\mathbf{Q}$ is expressed by a sum of the reciprocal-lattice vector $\mathbf{h}$ and the wave vector $\mathbf{q}$. For $\mathbf{q}\cdot\mathbf{u}_m \ll 1$ the scattered amplitude then can be written[16] as

$$\begin{aligned}\mathbf{F}(Q)&\approx\sum_m f_m \exp(i\mathbf{q}\cdot\langle \mathbf{R}_m \rangle)(1+i\mathbf{h}\cdot\mathbf{u}_m)\\ &=F_{\text{Bragg}}(Q)+F_{\text{Huang}}(Q)\ . \end{aligned} \quad (4)$$

For small defect numbers c the diffusely scattered intensity due to the displaced atoms is described by[11]

$$\begin{aligned}I_{\text{Huang}}(\mathbf{Q})&=c\left|if\mathbf{h}\cdot\sum_m \mathbf{t}(\mathbf{R}_m)\exp(i\mathbf{q}\cdot\langle \mathbf{R}_m \rangle)\right|^2\\ &=c|if\mathbf{h}\cdot\mathbf{T}(\mathbf{q})|^2\ . \end{aligned} \quad (5)$$

Here the individual displacements $\mathbf{u}_m$ are replaced by an average displacement field $\mathbf{t}(\mathbf{R})$. $\mathbf{T}(\mathbf{q})$ can be regarded as the Fourier transform of $\mathbf{t}(\mathbf{R})$. f is the mean structure factor of the crystal.

Due to the different atomic form factors of the defects and the lattice atoms one gets an additional antisymmetric part of the diffuse scattering. This originates from an interference between the scattering from the defects themselves and the scattering from the displaced atoms far away from the defects:

$$I_{\text{diffuse}}(\mathbf{Q})=I_{\text{Huang}}(\mathbf{Q})+I_{\text{anti}}(\mathbf{Q})\ . \quad (6)$$

The symmetric part is proportional to q^{-2}, while the antisymmetric part is proportional to q^{-1}.

Far away from the Bragg position the approximation mentioned above is no longer valid, because the condition $\mathbf{q}\cdot\mathbf{u} \ll 1$ is violated. In this limit the diffuse intensity decreases even faster, the symmetric part is proportional to q^{-4} (Stokes-Wilson scattering), while the antisymmetric part is proportional to q^{-3}. The crossover from Huang scattering to Stokes-Wilson scattering takes place at q_0, which can be associated with the defect size within the volume theory: $R_0=1/q_0$ is the mean radius of the defect.[1]

Taking into account the resolution of the diffractometer, the symmetric part of the diffuse scattering parallel to the reciprocal-lattice vector $\mathbf{h}$ can be written as[1]

$$I_{\text{symm}}=\begin{cases} C(1/q)\arctan(\Delta q_v/q) & \text{for } q<q_0\ ,\\ C(q_0^3/q^4)\arctan(\Delta q_v/q) & \text{for } q\geq q_0\ , \end{cases} \quad (7)$$

with

$$C=c(fh/v)^2\sum_{i=1}^{3}\gamma^i\pi^i\ . \quad (8)$$

Δq_v is the vertical resolution of the diffractometer. v is the mean volume of the atoms; γ^i and π^i are constants depending on the elastic constants of the crystal, the orientation and form of the defect, and direction of $\mathbf{q}$. A more detailed discussion of these constants can be found in Refs. 8 and 10.

III. SAMPLES

In this paper measurements with four GaAs crystals prepared differently are reported. For the sample preparation we used commercially available, polished GaAs($\bar{1}\bar{1}\bar{1}$) wafers. GaAs is a crystal with zinc-blende structure, its space group is $F\bar{4}3m$. The lattice constant is $a=5.653\,15$ Å and the mass density is $\rho=5.316$ g/cm^3.[17] For a face-centered-cubic structure like GaAs, there are three independent elastic constants whose values are listed in Table I.

On the ideal (111) surface, the topmost layer consists of Ga atoms; on the ideal ($\bar{1}\bar{1}\bar{1}$) surface it consists of As atoms. However, the real surfaces usually are reconstructed with a reconstruction mechanism depending on the preparation conditions. Properly prepared (111) surfaces show a 2×2 reconstruction only.[18] For x-ray crystallography the two orientations are equivalent, but for other spectroscopic methods that are sensitive to the electronic structure, such as photoemission or inverse photoemission, the orientations are different.

To show the effect of the different stages of a surface treatment [with the aim of getting a good GaAs(111) surface] we took an untreated GaAs($\bar{1}\bar{1}\bar{1}$) wafer as reference (sample A).

As a first step the unpolished backside of the wafers ([111] direction) is polished with diamond rubbing paste. A granulation down to 0.25 μm has been used. (111) wafers must not be etched, since wafers etched in a mixture of bromine and CH_3OH show etching holes on the (111) face.[19] Sample B is a GaAs wafer treated in this

TABLE I. The three elastic constants for fcc GaAs in Voight notation [T. B. Bateman, H. J. McSkimin, and J. M. McWhelan, J. Appl. Phys. **30**, 544 (1959)].

c_{11}	$(1.188\pm0.002)\times10^{11}$ N/m^2
c_{12}	$(0.538\pm0.003)\times10^{11}$ N/m^2
c_{44}	$(0.594\pm0.001)\times10^{11}$ N/m^2

way. The other two wafers with a size of 7×8 mm^2 have been prepared similarly. The latter are used as substrate for the MBE-grown samples. The MBE growth presents a more complex preparation which is described below. The wafers are built into a MBE system equipped with two evaporation sources, one for gallium and one for arsenic (As_4). The pressure in the UHV chamber is in the 10^{-10}-mbar range except for preparation. The samples are cleaned with 800-eV argon ions during several hours.

The MBE growth is performed with a ratio of As_4 to Ga flux of 2:1 and a substrate temperature of about 670 K. This gives rise to a growth rate of about 1500 Å/h. First, the substrate is heated only for 2 min to form a crystalline surface. During growth the quality of the epitaxial layer is controlled with a RHEED system. After stopping the MBE process by closing the source shutters and turning off the substrate heater, the sample is cooled down to 370 K and subsequently annealed at 720 K for several minutes.

The two MBE-grown samples have been treated differently so both preparations must be described.

(a) Sample C was ion bombarded for 3 h and MBE was done for 90 min followed by annealing for 10 min. This treatment yields a 2×2 reconstructed surface.

(b) Sample D was treated in three different cycles of ion bombardment, MBE, and annealing. In the first cycle no annealing after growth took place, in the second cycle the sample was only ion bombarded and annealed, and in the third cycle the same procedure as used for sample C was applied. In all cases a 2×2 reconstruction was observed with RHEED.

IV. EXPERIMENTAL SETUP

The experimental setup of the three-crystal diffractometer (TCD) is schematically shown in Fig. 1. The x-ray source is a 12-kW x-ray generator with a rotating copper (Cu) anode. Cu $K\alpha$ radiation is extracted by use of Bragg reflection from a flat Ge(111) crystal as monochromator. Slits of dimensions 10×0.1 mm^2 in front of and behind the monochromator limit the divergence of the beam so that only the $K\alpha_1$ part of the Cu radiation with wavelength $\lambda = 1.540\,56$ Å reaches the sample. Behind the sample a flat Ge(311) crystal is mounted as analyzer. A NaI scintillation counter serves as a detector. Lead shields around the monochromator and the detector system reduce the background radiation.

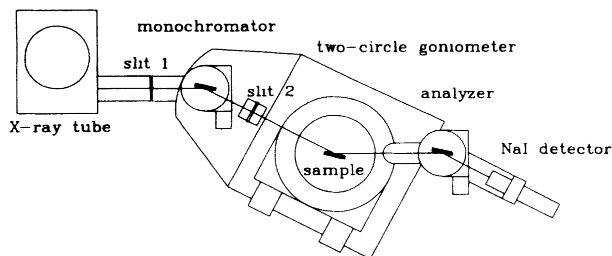

FIG. 1. Schematic drawing of the three-crystal diffractometer.

The use of a TCD to examine the defect concentration of samples has several advantages. With Δq values of $(1.0 \pm 0.1) \times 10^{-3}$ Å^{-1} parallel and $(1.8 \pm 0.1) \times 10^{-4}$ Å^{-1} perpendicular to the scattering vector **Q** within the scattering plane, the instrumental resolution of a TCD is rather high. The resolution is determined from the intensities at full width at half maximum (FWHM) of the reciprocal-lattice point 111 of a Ge(111) single crystal. In contrast to mosaic crystals, perfect single crystals reflect only within a small range of incident angles. This range is approximately equal to the width of the Darwin curve of the ideal single crystal. The resolution of the instrument perpendicular to the scattering plane Δq_v is more than 10 times poorer than the resolution in the scattering plane.

The analyzer crystal in front of the detector allows energy-resolved measurements. So the elastically scattered intensity can be separated and the inelastically scattered intensity, such as Compton scattering, is reduced to a minimum. Thermal diffuse scattering is not suppressed because the energies of the phonons are smaller than the energy resolution of the diffractometer.[20] The thermal diffuse scattering remains nearly unaffected by changes of the defect concentration.[21] It will be determined in the reference measurement and then subtracted. So, rather precise measurements of the Huang scattering and the Stokes-Wilson scattering become possible even at room temperature.

The background—for example, from air scattering—is also reduced because the analyzer crystal accepts only a narrow angular range. So it is possible to register weak scattered intensity as originating from point defects in a crystal.

The main disadvantage of a TCD is its complicated resolution function. The acceptance angles of the several crystals yield a "resolution star."[22] Figure 2 shows the contours of equal intensity for a Ge(111) single crystal for the reciprocal-lattice point 111. It is an example for such a "resolution star" for intensities in the 10^{-4}–10^{-6} range

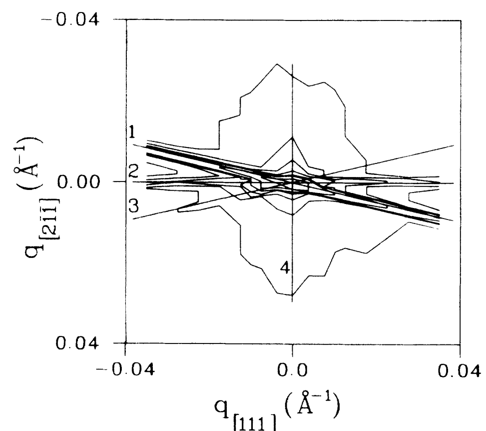

FIG. 2. "Resolution star" at the reciprocal-lattice point 111 of a Ge(111) single crystal. The lines denote the several streaks: 1, monochromator; 2, wavelength deviation; 3, analyzer; 4, mosaic spread.

relative to the intensity of the Bragg reflection. Two additional streaks stem from a mosaic spread of the sample and the wavelength distribution. Theoretical expressions for the "standard" resolution function of a three-crystal diffractometer are given by Cowley.[23] As a consequence, reference measurements are absolutely necessary to get information about the diffuse scattering. For this purpose, a measurement ($\theta/2\theta$ scan) near the reciprocal-lattice point $\bar{1}\bar{1}\bar{1}$ of the GaAs($\bar{1}\bar{1}\bar{1}$) sample has been performed.

V. MEASUREMENTS AND DISCUSSION

A. Determination of the diffuse scattering

To determine the diffuse scattering intensity we need an ideal sample as a reference; this means an undistorted crystal with a perfectly flat surface. The reference sample A used for these measurements does not fulfill these requirements completely. The defect concentration in this sample is probably low enough, but the sample shows strong diffuse scattering with a preferred orientation along the $(0\bar{1}1)$ reciprocal-lattice vector (see Fig. 6). From the "resolution star" we know that the intensity in this direction is affected by the mosaic spread of the sample. Although we examine more or less perfect single crystals the surface part of the crystals might resemble that of a mosaic crystal. This may result from a macroscopic roughness of the surfaces. Measurements at small angles—that is, near the critical angle of total external reflection—support this statement. The rocking curves (θ scans with 2θ fixed) performed in this region *have a width of several degrees.* Although the manufacturer has polished the wafer, there may be a wavelike fluctuation with long wavelength on the surface. Furthermore, the surface direction can only be defined within a degree (during the preparation procedure), so that a high-indexed surface normal and, consequently, a stepped surface also seems possible. For small diffraction angles this has the same effect as a high roughness because the beam illuminates the whole sample and averages over the illuminated area.

Therefore we cannot use anything but Bragg scans ($\theta/2\theta$ scans) for a determination of the diffusely scattered intensity. Although the Bragg scans are influenced by this roughness too, its effect is sufficiently small not to influence the conclusions about defects.

Additional diffuse scattering into the direction of the surface normal may be caused from Bragg scattering at the semi-infinitive crystal terminating at the surface, the so-called crystal truncation rods (CTR's).[24] The intensity of the CTR varies like q^{-r} with $2 \le r < 4$, the particular value of r depending on the roughness of the surface. For samples A and C, $r \approx 2.9$ and, for samples B and D, $r \approx 3.1$ have been found. This means that the intensity decrease for samples B–D is comparable or higher than for sample A used as reference. But the absolute scattering intensities of samples B–D are notably higher in the region of interest than that of sample A (see Fig. 3). This is not characteristic of CTR's. In addition, scans perpendicular to the direction of the surface normal have a width which is much broader than the FWHM of the resolution function so that no CTR can be detected. Hence we may exclude crystal truncation rods as a possible reason for additional intensity.

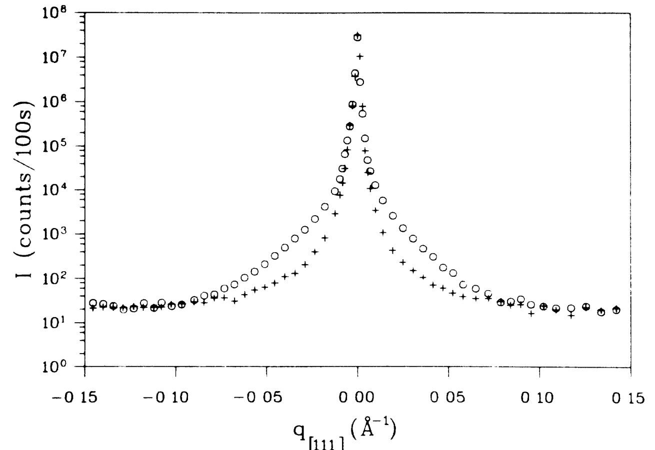

FIG. 3. Bragg scans for sample A [GaAs($\bar{1}\bar{1}\bar{1}$) wafer] and sample B [GaAs(111) wafer].

From the fact that the MBE samples only show additional diffuse scattering along the direction of the sample normal which coincides with the diffraction vector, we conclude that this diffuse scattering has its origin in the MBE layer. From defects in the bulk, one gets diffuse intensity which is isotropic around a reciprocal-lattice point. Only in the case of defects with high symmetry (for example, cubic defects) there may be a line or a plane of zero intensity which contains the reciprocal-lattice point.[4,8,11] Such high-symmetry defects seem rather improbable in our case. For silicon, e.g., which has nearly the same structure as GaAs, only defects with low symmetry[1,2,25] have been found. In our case the diffuse intensity only shows up in the direction of the surface normal with a small extension perpendicular to this direction. A situation similar to ours is treated in the calculations by Barabash and Krivoglaz.[14] According to them the above features are observed when the defects are limited to a near-surface region. A direct experimental decision between the different possibilities—the diffraction from the layers and the diffraction of the substrate—cannot be made: With the diffraction geometry used, the penetration depth of the x rays is much larger than the thickness of the layer.

B. Bragg scans

Figure 3 compares a Bragg scan of sample A (crosses) with one of sample B (dots), respectively, on a logarithmic scale. In the immediate vicinity of the Bragg reflection, these intensities are nearly identical, but for $|q| > 0.02$ Å^{-1} additional diffuse scattering of sample B is quite obvious. We subtract the "reference" intensity from the measured intensity to get the diffusely scattered intensity $I_{\rm diff} = I_{\rm meas} - I_{\rm ref}$ and then calculate the symmetric part of the diffusely scattered intensity $I_{\rm symm} = [I_{\rm diff}(+q) + I_{\rm diff}(-q)]/2$, which is shown in Fig.

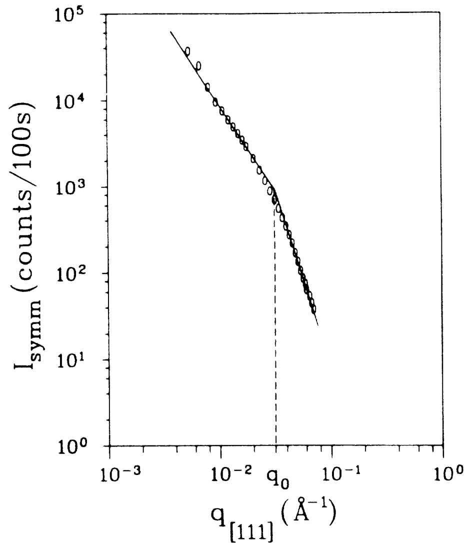

FIG. 4. Symmetrical part of diffusely scattered intensity for sample B [GaAs(111) wafer] on a double-logarithmic scale.

4. The solid line represents the theoretical model [Eq. (7)] fitted to the data. At the point q_0 a transition takes place from the q^{-2} dependence of the Huang scattering to the q^{-4} dependence of the Stokes-Wilson scattering. This point close to the Bragg reflection indicates the occurance of defect clusters.[1] Due to the heat treatment during MBE the defects have a high mobility within the layer and may form areas with a high concentration of defects. These are usually denoted as defect clusters. From the value q_0 extracted from the fit of the model to the experiment, we get the cluster radii of the defects (see Table II). The measurements give cluster radii from 31.5 Å up to 49.5 Å. These values are rather high; there are approximately 10 000 atoms in such clusters. Assuming one defect per unit cell (eight atoms) there are about 1000 defects in a cluster. On the other hand, this would explain the observed high diffusely scattered intensity, since it is directly proportional to the number of defects in the cluster.[11]

For the fit the data points near q_0 have not been included because the model is not valid near this point. Data points with an intensity less than one count per 100 s have been neglected too, because the counting statistics were insufficient.

There is another aspect concerning the MBE-grown layers. Due to the defects the density ρ_{MBE} of these GaAs layers is different from the density ρ_{bulk} of the GaAs substrate. So in analogy with the Kiessig fringes in the region of total external reflection[26] one gets a modulation of the intensity near the Bragg reflection. It originates from a superposition of waves reflected at the surface and waves reflected at the interface between the layer and the substrate (see Fig. 5). The dots represent the observed intensities. The solid line results from a simple kinematical calculation done by summing incoherently over the substrate Bragg scattering and the Bragg scattering of the MBE layer. Concerning the lattice constant of the MBE layer, we allow for a small departure from the predicted value. As corrections we take into account only the absorption of the x rays and the finite q resolution of the experimental setup. Table III shows the results for the thicknesses and the lattice parameters.

The thickness of the MBE layer of sample C is found to be 3330±70 Å and of sample D 2900±40 Å. This is in rather good agreement with the quartz-oscillator measurements performed during MBE growth.

Additional information about the defects can be obtained from the antisymmetric part of the diffuse scattering[8,11] $I_{anti}=[I_{diff}(+q)-I_{diff}(-q)]/2$. For sample B the antisymmetric part is positive for $\mathbf{q}\cdot\mathbf{h}<0$ and for samples C and D the antisymmetric part is positive for $\mathbf{q}\cdot\mathbf{h}>0$. So the defects in sample B may be vacancies perhaps due to the surface treatment. For the MBE samples the defects seem to be interstitials.[1] This may result from an excess supply of arsenide in the vacuum chamber during the growth. There may also be vacancies in the MBE layers, especially in the interface between the substrate to the layer, but we cannot separate the diffuse scattering of the vacancies, because the scattering strength of the vacancies is much smaller than the scattering strength of the interstitials.

One should note that there is a great difference in the q dependence of the anitsymmetric part of the scattering from sample B and that of samples C and D. The antisymmetric part of the diffuse scattering of sample B shows a similar behavior as its symmetric part. Near the position of the Bragg reflection the antisymmetric part is proportional to q^{-1}; beyond $\tilde{q}_0=0.0267\pm0.0005$ Å^{-1}

TABLE II. The crossover points q_0 of the symmetric part of the diffusely scattered intensity to evaluate the cluster radii and the number of defects in the cluster (see text).

Sample	q_0 (Å^{-1})	R_0 (Å)	n_{cl}
B	0.0318±0.0003	31.5±0.3	700
C	0.0202±0.0016	49.5±4.2	2800
D	0.0279±0.0007	35.8±1.2	1000

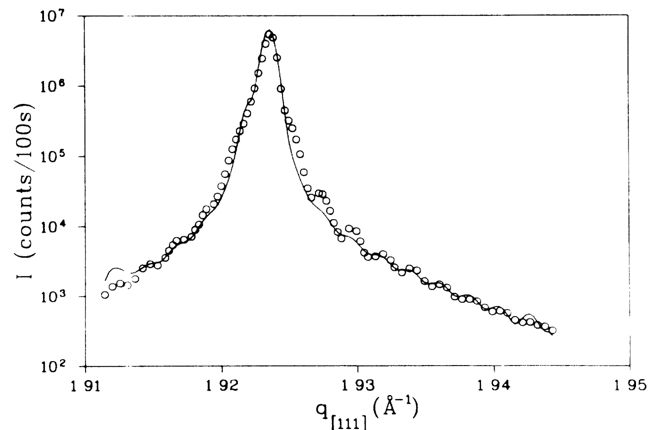

FIG. 5. Kiessig fringes observed at the reciprocal-lattice point 111 for sample D [GaAs(111) MBE layer on GaAs(111) wafer]. The solid line is calculated with kinematical theory.

TABLE III. Evaluated lattice parameters and thicknesses of the MBE layers.

Sample	a (Å)	d (Å)
C	5.654 72±0.0015	3330±70
D	5.654 14±0.0009	2900±40

the intensity decreases with q^{-3}. The crossover point $\tilde{q}_0$ of the antisymmetric part of the scattering, however, shows a notable deviation from that of the symmetric part of the scattering. Samples C and D show a different behavior. The antisymmetric part is much stronger than for sample B and the decrease is proportional to q^{-3} over the whole q range.

Additional information can be extracted from the shift of the position of the Bragg reflection due to the defect-induced atomic diplacements. The observed lattice-parameter changes are listed in Table IV. These lattice-parameter changes are in fairly good agreement with the values obtained from the separation of the maxima of the Kiessig fringes (see Table III).

The lattice-parameter change is connected to π^1 via[3]

$$\frac{\Delta a}{a} = c n_{\rm cl} \frac{(\pi^1/3)^{1/2}}{v_c(c_{11}+2c_{12})} .$$

$n_{\rm cl}$ is the mean number of defects in a cluster and v_c is the volume of the unit cell. We can only calculate $c(\pi^1)^{1/2}$ (see Table IV). $(\pi^1)^{1/2}$ typically has a value of several eV, so we can estimate the concentration of the defect clusters to be several parts per million.

From the theory of diffuse scattering from defects,[11] additional information about the defects could be obtained from the static Debye-Waller factor due to the static displacement of the atoms, but within the experimental error the expected decrease of the intensity of the Bragg reflection was not observed. At the same time, no broadening of the peaks could be seen. These results are compatible with the theory of diffuse scattering from defects in thin films,[14] where Debye-Waller factors near unity are predicted. This is another hint that the diffuse scattering is produced from near-surface defects and not from defects in the bulk.

C. Isointensity contour scans

To determine the diffuse scattering around the reciprocal-lattice point 111, we made rocking scans at different detector positions with a q range of ± 0.06 Å^{-1} in the $[0\bar{1}1]$ direction and a range of ± 0.04 Å^{-1} in the [111] direction (the region of the first Brillouin zone). The isointensity contour plots for samples A, B, and D are shown in Figs. 6–8. For sample A the diffuse scattering is extending in all directions, strongest in the direction of the mosaic spread. The same observation is made for sample B, but there the diffusely scattered intensity is more concentrated in the directions of the streaks. For the MBE-grown samples C and D the situation is different. Sample C shows the same features as sample D and therefore the latter is presented.

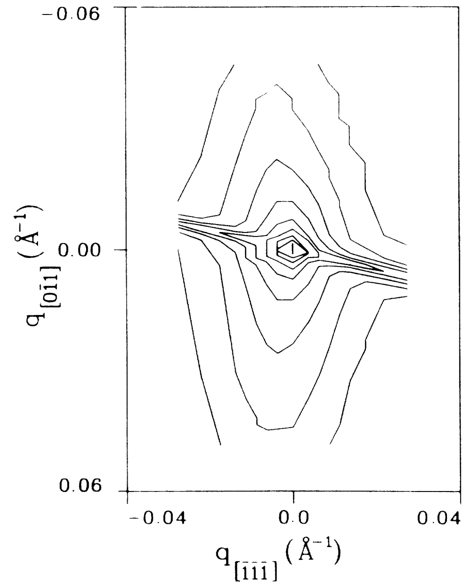

FIG. 6. Isointensity contour plot for sample A [GaAs($\bar{1}\bar{1}\bar{1}$) wafer], $I = 10^x$ counts/s, $x \in \{0, 0.5, 1, 1.5, 2, 2.5, 3, 3.5, 4\}$.

For samples C and D two additional streaks are running diagonally through the reciprocal space. They form angles of nearly 66.5° and 111.6°, respectively, with the [111] direction. These streaks do not coincide with high-symmetry directions in reciprocal space. Similar streaks have already been observed with neutron scattering in Czochralski-grown dislocation-free silicon single crystals after heat treatment.[6] Messoloras *et al.* explain this diffuse scattering with small amorphous SiO_2 precipitates, but a satisfactory explanation of our experimental findings is still missing. Both MBE-grown samples show this phenomenon, although the surface treatments were different.

TABLE IV. Measured lattice parameters and relative lattice parameter changes to the nominal value.

Sample	a (Å)	$\Delta a/a$	$c(\pi^1)^{1/2}$ (N/m)
B	5.6543±0.0004	$(2.11\pm1.27)\times10^{-4}$	$(1.6\pm0.6)\times10^{-23}$
C	5.6564±0.0004	$(5.77\pm1.52)\times10^{-4}$	$(0.7\pm0.2)\times10^{-23}$
D	5.6550±0.0002	$(3.22\pm0.78)\times10^{-4}$	$(1.1\pm0.3)\times10^{-23}$

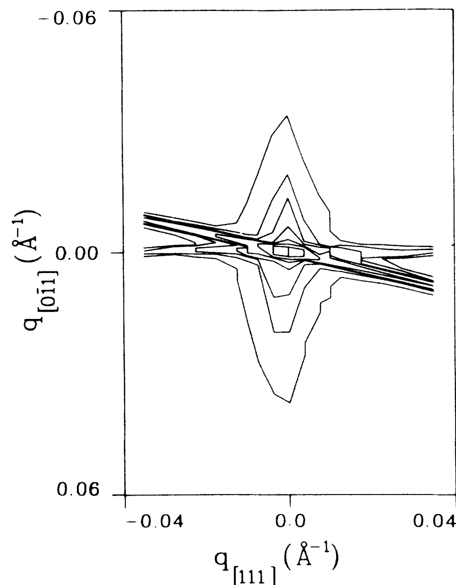

FIG. 7. Isointensity contour plot for sample B [GaAs(111) wafer], $I = 10^x$ counts/s, $x \in \{0, 0.5, 1, 1.5, 2, 2.5, 3, 3.5, 4\}$.

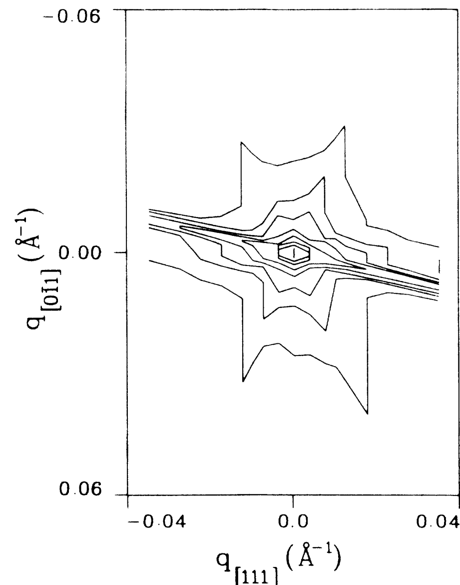

FIG. 8. Isointensity contour plot for sample D [MBE layer on GaAs(111) wafer], $I = 10^x$ counts/s, $x \in \{0, 0.5, 1, 1.5, 2, 2.5, 3, 3.5, 4\}$.

VI. CONCLUSIONS

From x-ray-diffraction measurements near Bragg reflection we observe pronounced diffuse scattering. A crystal truncation rod is not observed. The diffuse scattering is concentrated in small streaks along the reciprocal-lattice vector **Q** normal to the surface, so that we can conclude that the diffuse scattering is produced by defects either in a near-surface region or in a thin MBE layer with a thickness of nearly 3000 Å. Defect clusters with nearly 30 Å diameter are found. For the MBE-grown layers two additional streaks have been identified which probably originate from the defects in the MBE-grown layers.

The samples have a relatively high roughness, which may come from both a stepped surface and the influence of oxidation. This problem is not solved yet. In order to clarify the situation, we plan to make x-ray measurements, in UHV. Then we can exclude the influence of oxygen and other contaminations or expose the sample to a well-defined oxiding atmospere. This will allow us to investigate a wafer over all stages of production from polishing over sputtering to the resulting MBE-grown layer without a disturbing outer influence. Then it shall be possible to examine the effect of oxygen on the surface.

Additional information about roughness and surface reconstruction can be obtained through measurements of the crystal truncation rods[24] and, in particular, with grazing-incidence diffraction measurements[25] using synchrotron radiation, as planned.

[1] W. Mayer and H. Peisl, J. Nucl. Mater. **108&109**, 627 (1982).
[2] D. Bahr, L. Brügemann, P. Dreier, and W. Press (unpublished).
[3] P. Ehrhardt and W. Schilling, Phys. Rev. B **8**, 2604 (1973).
[4] B. C. Larson and W. Schmatz, Phys. Rev. B **10**, 2307 (1974).
[5] S. Yasuami, J. Harada, and K. Wakamatsu, J. Appl. Phys. **50**, 6860 (1979).
[6] S. Messoloras, J. R. Schneider, R. J. Stewart, and W. Zulehner, Semicond. Sci. Technol. **4**, 340 (1989).
[7] M. A. Krivoglaz, *Theory of X-ray and Thermal-Neutron-Scattering by Real Crystals* (Plenum, New York, 1969).
[8] H. Trinkaus, Phys. Status Solidi B **51**, 307 (1972).
[9] H. Trinkaus, Phys. Status Solidi B **54**, 209 (1972).
[10] P. H. Dederichs, Phys. Rev. B **4**, 1041 (1971).
[11] P. H. Dederichs, J. Phys. F **3**, 471 (1973).
[12] S. Dietrich and W. Fenzl, Phys. Rev. B **39**, 8873 (1989).
[13] S. Dietrich and W. Fenzl, Phys. Rev. B **39**, 8900 (1989).
[14] R. I. Barabash and M. A. Krivoglaz, Fiz. Tverd. Tela (Leningrad) **29**, 3081 (1987) [Sov. Phys.—Solid State **29**, 1768 (1987)].
[15] S. Grotehans, G. Wallner, E. Burkel, H. Metzger, J. Peisl, and H. Wagner, Phys. Rev. B **39**, 8450 (1989).
[16] D. T. Keating, J. Phys. Chem. Solids **29**, 771 (1968).
[17] *Handbook of Chemistry and Physics*, 66th ed., edited by R. C. Weast (Chemical Rubber Co., Boca Raton, 1986).
[18] M. Alonso, F. Soria, and J. L. Scadon, J. Vac. Sci. Technol. A **3**, 1598 (1985).
[19] J. van Bommel and J. E. Crombeen, Surf. Sci. **13**, 437 (1976).
[20] B. T. M. Willis and A. W. Pryor, *Thermal Vibration in Crystallography* (Cambridge University Press, London, 1975).
[21] E. Eisenriegler, Cryst. Lattice Defects **2**, 181 (1971).
[22] T. Ryan, Ph.D. thesis, University of Edinburgh, 1987.
[23] R. A. Cowley, Acta Crystallogr. Sect. A **43**, 825 (1987).
[24] I. K. Robinson, Phys. Rev. B **33**, 3830 (1985).
[25] B. C. Larson and J. F. Barhorst, in *Defects in Semiconductors*, edited by J. Narayan (North-Holland, Amsterdam, 1981).
[26] F. Rieutord, J. J. Benattar, L. Bosio, P. Robin, C. Blot, and R. de Kouchkovsky, J. Phys. (Paris) **48**, 679 (1987).